J. Fluid Mech. (1974), *vol.* 65, *part* 2, *pp.* 247–260
Printed in Great Britain

Natural convection in a shallow cavity with differentially heated end walls. Part 3. Experimental results

By JORG IMBERGER

Departments of Mathematics and Mechanical Engineering, University of Western Australia, Nedlands

(Received 24 May 1973)

The steady motion of water in an enclosed rectangular cavity with differentially heated vertical end walls was studied experimentally, and the results are compared with the findings of parts 1 and 2. The depth-to-length ratios of the cavities were 10^{-2} and $1{\cdot}9 \times 10^{-2}$, and the Rayleigh number was allowed to vary sufficiently to enable a study to be made of the transition from a flow driven by the vertical wall boundary layers to one sustained by a longitudinal temperature gradient in the central sections of the cavity.

1. Introduction

One feature of a well-mixed estuary is the presence of a horizontal density gradient, often linear and independent of the vertical position over large reaches of the estuary. This situation is especially prevalent when the depth of the estuary is very much smaller than its length and the mixing in the estuary is sufficient to prevent definite density wedges from forming. Logan & Cebulski (1970) measured salinities in Shark Bay on the West Australian coast and their data give perhaps the most graphic illustration of such a density gradient. The slow horizontal and transverse gravitational circulations induced by these density gradients have been shown, by Fischer (1972), to contribute a major part of the longitudinal dispersion of pollutants in an estuary.

The time scale of the gravitational circulation is rather large, so that the motion is coupled to any tidal or other unsteady variations of velocity in the estuary only through effective eddy exchange coefficients. A qualitative description of the physical mechanism of the slow gravitational circulation may thus be obtained by examining a laminar flow model. In view of this it was decided to investigate the flow in a long shallow cavity with differentially heated vertical end plates. However, it was soon found that the energy stored in a surface film was larger than the buoyancy energy being supplied to the water. Slight changes in the surface tension would induce velocity variations larger than those to be measured. It was therefore decided to eliminate this uncertainty by placing the upper insulating ceiling in contact with the water surface. In part 1 of this series Cormack, Leal & Imberger (1974) investigated the analytical consequences of the limit of a small depth-to-length ratio, while in part 2 Cormack, Leal &

Seinfeld (1974) developed an algorithm for the numerical solution for the flow in such a shallow cavity. The present part reports the results of an experimental investigation of the transition from a flow driven mainly by a longitudinal core temperature gradient to one which is propelled by the momentum gained from the buoyancy forces in the vertical layers. The properties of the flow associated with these two types of motion and the transition between them have been elucidated in parts 1 and 2 and these are found to agree with the present experimental findings. A future paper will report on the three-dimensional circulation induced in a cavity with a transversely sloping bottom.

The first experimental investigations of flow in cavities of unit and large aspect ratios were carried out by Eckert & Carlson (1961), who demonstrated that the flow in a cavity of a given aspect ratio was steady up to a certain value of the Grashof number, but thereafter was unstable. Elder (1965) showed that before the onset of fully developed turbulence there was an intermediate steady motion composed of horizontal rolls. Hart (1971) extended this investigation to include the effects of the angular orientation of the cavity, and recently Jannot & Mazeas (1973) reconsidered the problem dealt with by Elder (1965), and gathered further data on the correlation between the Nusselt number and the Rayleigh number in the laminar, transitional and turbulent regimes. However, to the author's knowledge no investigation, to date, has dealt with the steady flow in a cavity of small aspect ratio.

2. Experimental apparatus

The experimental apparatus is depicted schematically in figure 1(*a*). The water is contained in an insulated long Plexiglas box, the vertical end walls of which are kept at different constant temperatures. The depth h and the temperature differential ΔT applied across the end walls were the experimental variables. All told a series of eight separate experiments was conducted in which the Rayleigh number Ra changed by a factor of 100 and the aspect ratio A by a factor of 2. The critical parameter Ra^2A^3, discussed in part 1, ranged from about 10^6 to 10^{11}. A summary of the experimental parameters is given in table 1.

The experiments were carried out in a 258·5 cm long, by 45 cm wide tank, made from 2 cm thick Plexiglas. The construction of the tank allowed the position of the upper surface to be adjusted, permitting continuous variation of the depth of the cavity up to 6 cm. This was achieved by hanging the lid from cross-members supported on the edges of the vertical side walls. By adjusting the set screws at the supports, the upper surface could be positioned and levelled very accurately. The gap between the sliding lid and vertical walls was less than 1 mm. The upper and lower horizontal surfaces were insulated against heat losses by being enclosed in a second Plexiglas shell with a 4 cm air gap between the cavity wall and the outer shell. To prevent longitudinal convective transfer of heat in the air gap this was broken into small sections by inserting Styrofome strips transversely every 30 cm. This second insulation was not added to the side walls, where it was felt that the heat losses would be small, and where a fog-free surface was required for photography of the dye lines. The ends of the cavity consisted of stainless-steel

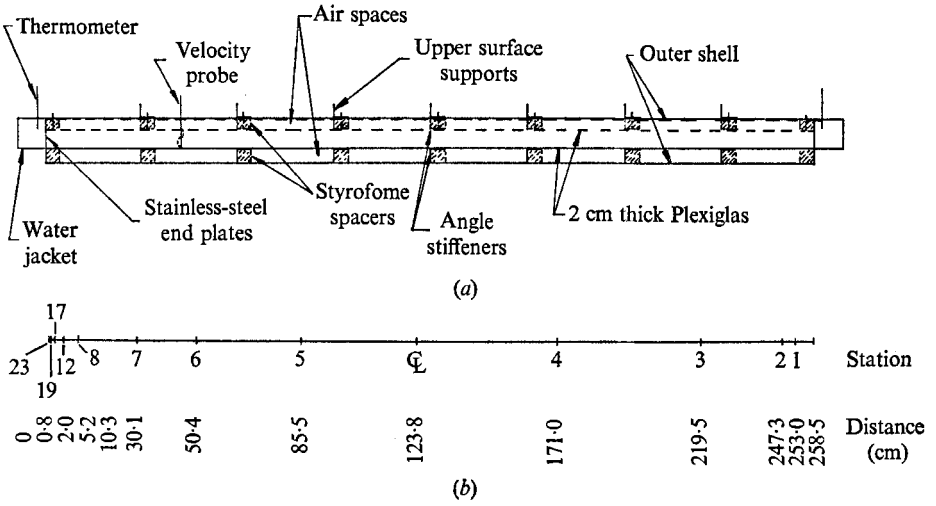

FIGURE 1. (*a*) General layout of experimental cavity and (*b*) position of measuring stations.

Experiment	h (cm)	ΔT (°C)	Ra	$Ra^2A^3 = Gr^2Pr^2A^3$	$K_1 = KL/\Delta T$	$\overline{Nu}A - A$
4	4·95	2·9	$8{\cdot}04 \times 10^6$	$4{\cdot}35 \times 10^8$	0·21	8·15
2	4·90	5·0	$1{\cdot}41 \times 10^7$	$1{\cdot}34 \times 10^9$	0·16	12·8
1	4·90	10·4	$3{\cdot}35 \times 10^7$	$7{\cdot}34 \times 10^9$	0·08	16·3
3	5·00	22	$1{\cdot}11 \times 10^8$	$8{\cdot}01 \times 10^{10}$	0·05	23·4
5	2·65	2·5	$1{\cdot}31 \times 10^6$	$1{\cdot}72 \times 10^6$	0·75	1·23
6	2·65	5·0	$2{\cdot}34 \times 10^6$	$5{\cdot}50 \times 10^6$	0·58	2·14
7	2·65	9·9	$3{\cdot}34 \times 10^6$	$2{\cdot}26 \times 10^7$	0·40	4·07
8	2·65	19·0	$1{\cdot}22 \times 10^7$	$1{\cdot}50 \times 10^8$	0·28	8·38

Constants: $L = 258{\cdot}5$ cm, $b = 45$ cm, $Pr = 7{\cdot}0$

TABLE 1. Values of experimental parameters

sheets backed by a water jacket. Hot and cold water was fed into these jackets by mixing the hot and cold water from the building's water supply. It was found that, although this procedure was somewhat wasteful, it was simple, and it yielded end temperature conditions which were constant to within $\pm 0{\cdot}1$ °C during the experiments. The end-wall temperatures were measured by immersing a precision thermometer in the water jackets. The insulation of the entire cavity was checked by measuring the temperature at the exact centre of the cavity and comparing this with the mean of the end-wall temperatures. It was found that provided that the room temperature was somewhere between the end-wall temperature extremes this centre-point temperature was equal to the mean temperature to within ± 2 % of the difference ΔT. The measurement probes could be inserted through very fine holes in the shell and upper surfaces at intervals along the centre of the tank as shown in figure 1 (*b*).

The temperature inside the cavity was obtained by measuring the resistance change of a thermistor probe with a digital ohm meter. A 0·5 mm diameter bead thermistor of nominal resistance 150 kΩ was mounted in a stiff teflon tube, which in turn was allowed to protrude from a stainless-steel tube. With a four-figure ohm meter temperatures could be accurately measured to within ± 0·02 °C. The probe was calibrated using a precision thermometer immersed in a thermos flask full of water. The calibration was repeatedly spot checked, but over the whole three-month period no noticeable drift was detected. To allow vertical positioning, the probe was mounted on a pinion-and-rack pointer gauge.

Velocity measurements were made using the pH indicator method proposed by Baker (1966). Thymol blue was mixed with the water and the solution was brought to the neutral point by adding sodium hydroxide until the solution was quite deep blue and then titrating hydrochloric acid into the mixture to restore the colour to a pale orange. The probe used to bring about a local change of colour was made from a piece of 0·25 mm straight steel piano wire. The wire was coated for lengths of 3 mm at intervals of 4 mm with a thin mixture of liquid tape and solvent. This proved an effective way of obtaining equally spaced uniform streaks of dye of thickness 1 mm which acted as streamlines. The spacing also provided a convenient way of determining the projection scale of the photographed dye images. The thickness of the probe was rather larger than that originally suggested by Baker (1966), but the added stiffness allowed easy positioning of the probe through the fine holes in the upper surface of the cavity. The velocity of the fluid could thus be obtained by photographing the dye images and noting the time which had elapsed since the electric current had been switched on.

The Reynolds number of the flow around the cylindrical probe ranged from zero to about one. This meant that there was a well-developed, but steady, wake behind the wire. The velocity of the leading tip of a typical dye line being formed at the probe could be seen to increase with distance from the probe, because the dyed fluid was caught in the wake of the wire. Therefore, the free-stream velocity to be measured could no longer be assumed to be given by the simple formula of distance divided by time elapsed. The probe was therefore calibrated at a number of Reynolds numbers by plotting the distance divided by the time elapsed against the distance from the probe. The asymptotic value of this velocity, for large distances from the probe, was used to calculate the actual Reynolds number. Actual velocity measurements could then be obtained by appealing to a Reynolds-number similarity, but an iterative approach was still required as the actual Reynolds number was not known. However, as most of the data had a dye streak length of $\frac{1}{4}$–$1\frac{1}{2}$ cm the correction factor varied only between 1·5 and 2·0 and an estimate of the true velocity to within ± 5 % could be obtained with one or two iterations.

In the end sections where the streamlines were no longer parallel or horizontal, the dye method was used to trace out streamlines rather than a velocity profile. The vertical probe was positioned well outside the end regions and a velocity profile was first taken. Then, the dye formation was allowed to continue long enough for the dye streaks to trace out streamlines throughout the whole region of interest. The value of the stream function associated with these streaks

was obtained by integrating the initial velocity distribution. In this way two checks could be carried out on the measuring technique. First, the net flow across the vertical cross-section must be zero. Second, at the hot end, where all the measurements were made, the fluid is moving towards the end wall at the lower depths and away from the wall back towards the probe near the top of the cavity. Hence, once a particular dye streak has been assigned a definite stream-function value, it must match up with this value on its return to the probe in the upper part of the cavity.

Throughout the experiment, the dye streaks were recroded photographically. The negative images were then projected and traced onto white graph paper. All times were determined with a stop watch.

3. Experimental results for the core flow

For the limit $A \to 0$, it was demonstrated in part 1 that the solution in the central region of the cavity is given by a parallel core flow. This core flow is driven by the hydrostatic pressure gradient set up by the linear density gradient in the longitudinal direction, and a counter uniform pressure gradient necessary for a zero net pressure gradient on any vertical cross-section. The temperature distribution is kept steady by vertical diffusion exactly balancing the horizontal convective transport of heat by the parallel flow moving through a longitudinal temperature gradient. The situation is essentially analogous to the mechanism proposed by Taylor (1954) for the longitudinal dispersion of an inert tracer in a shear flow, the only difference being that here the temperature gradients lead to density gradients which in turn provide the driving force for the flow.

Suppose that K °C cm^{-1} is the dimensional horizontal temperature gradient in the core region, then as shown in part 1, the velocity u and the temperature T are given by

$$u = (\beta g K h^3/\nu)\,(\tfrac{1}{6}\eta^3 - \tfrac{1}{4}\eta^2 + \tfrac{1}{12}\eta) \tag{1}$$

and

$$T - T_0 = Kx + (K^2\beta g h^5/D\nu)\,\{\tfrac{1}{24}\eta^3\,(\tfrac{1}{5}\eta^2 - \tfrac{1}{2}\eta + \tfrac{1}{3}) - \tfrac{1}{1440}\}, \tag{2}$$

where $D = k/c_P\rho_0$ and the remaining symbols have the same meaning as in part 1.

The aim of the experiments in the core region was to determine K from the experimental temperature measurements, and then to compare the experimental values of the velocity and the vertical variations of temperature with those predicted by (1) and (2). To do this the temperature data were plotted as a function of η for all the stations along the tank. Values of the temperature at $\eta = 0{\cdot}15$, $0{\cdot}5$ and $0{\cdot}85$ were then read off and plotted against the distance x from the hot end wall. Examples of such plots for the two depths studied and the two extreme temperature differentials are shown in figures 2(*a*), (*b*) and (*c*). It is seen that in the central part of the cavity there exists a region in which the longitudinal temperature gradient is linear and uniform with depth, although the length of this region decreases with increasing Ra^2A^3 until a state is reached, as shown in figure 2(*c*), where the region has completely disappeared. For cross-sections where the three temperature lines were parallel, a value of K was deter-

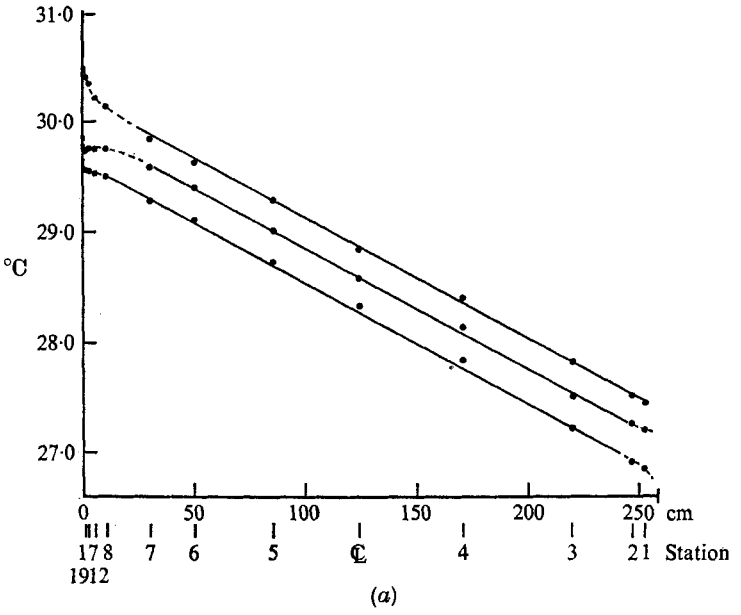

(*a*)

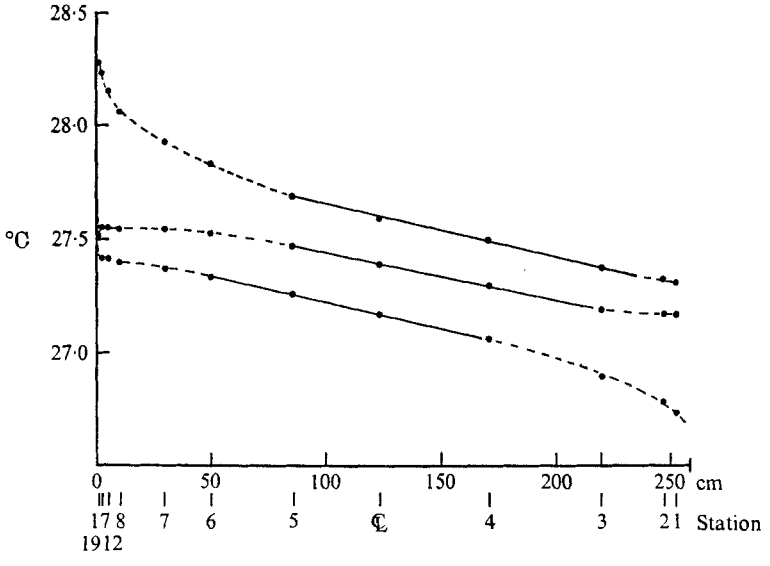

(*b*)

FIGURES 2(*a*, *b*). For legend see facing page.

mined by averaging the three gradients involved. All the velocity and temperature data originating from such cross-sections are plotted non-dimensionally in figures 3 and 4. The reduction of the temperature was modified in that the measured centre-line temperature T_c was used rather than the theoretical value $Kx - K^2\beta g h^5/1440 D\nu$. This was thought more realistic in view of the

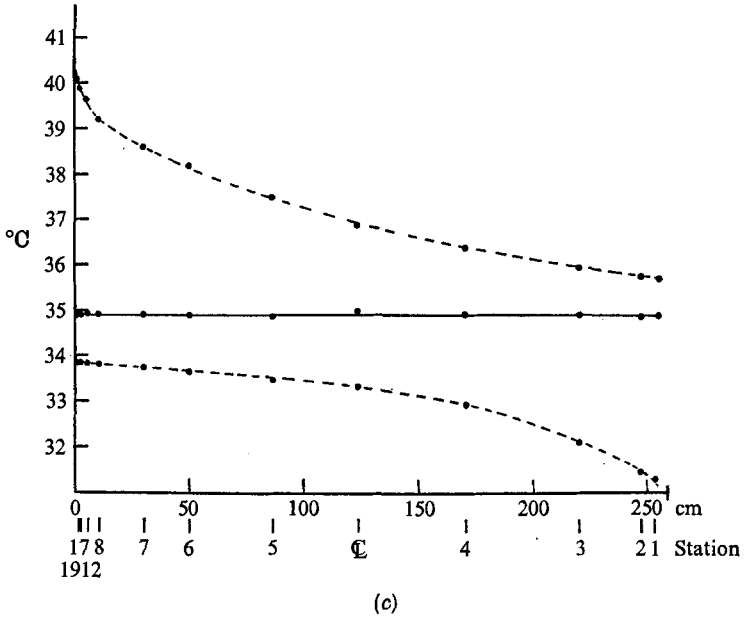

FIGURE 2. Temperature *vs.* horizontal distance from hot wall for $z/h = 0{\cdot}15$, $0{\cdot}50$ and $0{\cdot}85$. (*a*) Experiment 6: $Ra^2A^3 = 5{\cdot}50 \times 10^6$. (*b*) Experiment 4: $Ra^2A^3 = 4{\cdot}35 \times 10^8$. (*c*) Experiment 3: $Ra^2A^3 = 8{\cdot}01 \times 10^{10}$.

fifth-power involvement of h. The results are a strong verification of the parallel-flow theory. The deviation from the theory is indicated by a systematic outward trend at the top and bottom of the temperature curves and is due to the inclusion of some cross-sections which were no longer strictly self-similar. This departure is more noticeable near the outflowing levels of the flow since it is to these regions that the effect of the hot (or cold) end wall is convected. This is very clearly illustrated by the temperature distributions shown in figure 2, where the linearity associated with the core flow continues until the very close proximity of the end wall at the bottom of the hot plate or the top of the cold plate. Contrasted with this are the strong deviations from linearity associated with the outflowing regions. This phenomenon was also noticed in part 2.

The value of $KL/\Delta T$ is determined by the aspect ratio A, the Rayleigh number Ra and the Prandtl number Pr. The type of dependence on A, Ra and Pr originates from the coupling of the flow in the end regions and the core flow. For Ra fixed and $A \to 0$, this dependence may be deduced by systematically coupling the two regions via a perturbation analysis as was done in part 1, or by invoking the bulk conservation of heat transferred from the heated plate to the core flow, and noticing that a change in K requires temperature changes in the end region of order KL. Both methods yield the result that

$$K_1 = KL/\Delta T = 1 - O(Ra^2A^3).$$

Figure 5 is a plot of K_1 *vs.* Ra^2A^3, very similar to that shown in part 2, but with the experimental values added. The value of K_1 decreases from one at $Ra^2A^3 = 10^4$

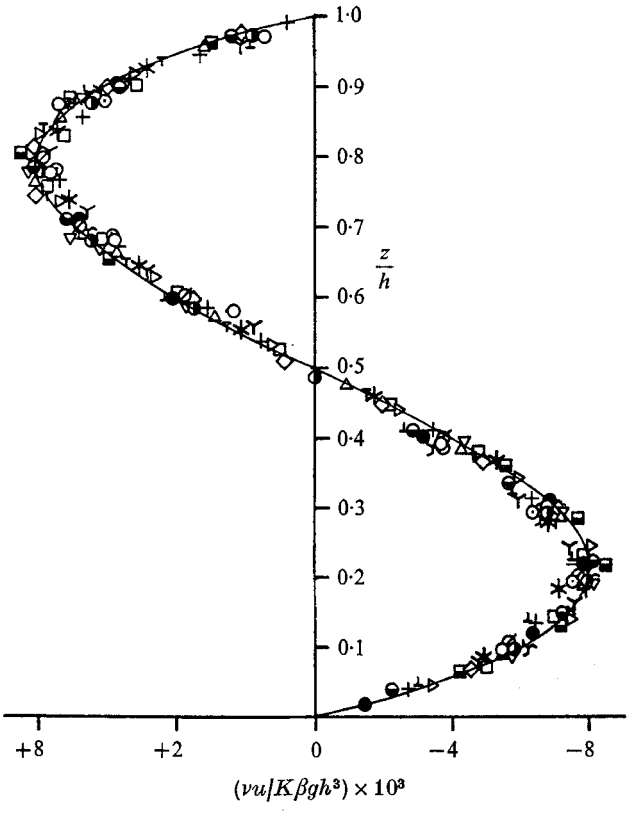

FIGURE 3. Non-dimensional velocity *vs.* distance above the bottom of the cavity. Results from all stations within regions of constant horizontal temperature gradient are included. ——, theoretical variation.

⌀	○	⊙	τ	●	Y	◒	◑	T	⊥	+	*	⊣	▽	△	▷	□	◇	⬓
Station																		
4	¢	5	4	¢	5	3	4	3	4	¢	5	7	4	¢	5	4	¢	5
Experiment																		
4	4	4	2	2	2	5	5	6	6	6	6	6	7	7	7	8	8	8

to nearly zero at $Ra^2A^3 = 10^{11}$. However as may be seen by comparing the data from part 2, computed for aspect ratios of 0·05, 0·1 and 0·2, and the present experimental data, taken at values of $A = 0{\cdot}01$ and 0·019, the two agree very well for Ra^2A^3 less than say 10^6, but there is a small, but systematic, deviation at larger values of Ra^2A^3. This is to be expected, and will be dealt with further in §§ 4 and 5. For large values of Ra^2A^3 the flow is no longer governed solely by the mechanisms outlined in part 1, but rather by a mechanism similar to that proposed by Gill (1966). The flow in the end regions now scales horizontally with $hRa^{-\frac{1}{4}}$, rather than h. At intermediate values of Ra^2A^3 both mechanisms are active and although there may still be a central portion of the cavity which contains parallel flow, the temperature gradient associated with this will no longer just scale with the combination Ra^2A^3, but also with A. In figure 5, the

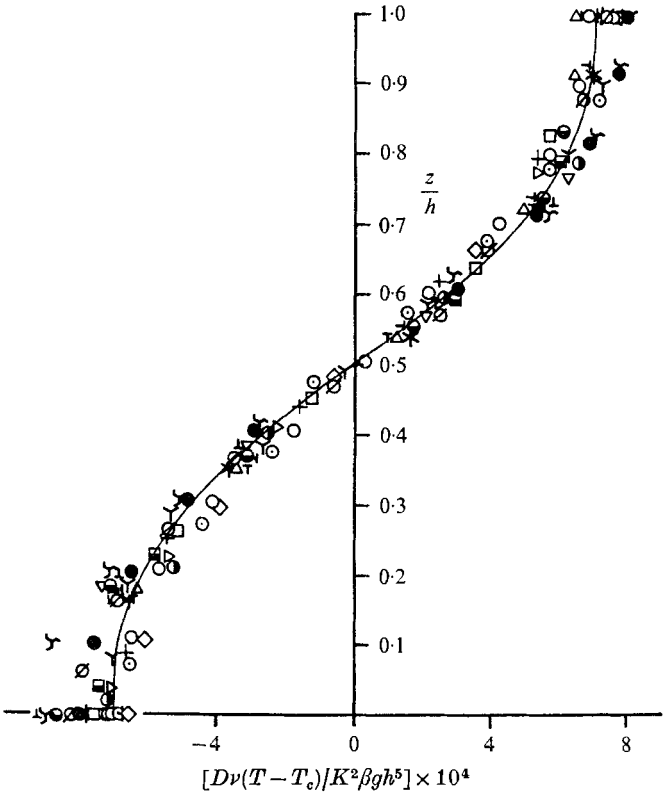

FIGURE 4. Non-dimensional temperature *vs.* distance above the bottom of the cavity. The measured mid-depth temperature T_c is used rather than the theoretical value

$$Kx-K^2\beta gh^5/1440D\nu.$$

Results from all stations within regions of constant horizontal temperature are included. Symbols as in figure 3.

results of experiments 1 and 3 have been included, but as is seen from figure 2 (*c*), the flow in the core is no longer parallel. The end regions have encroached all the way to the centre of the cavity. The value of Ra^2A^3 at which this happens clearly depends on the aspect ratio A. In part 2, where $A = 0{\cdot}1$, this occurred for $Ra^2A^3 = 10^6$, and in the experiments where $A = 0{\cdot}01$ and $0{\cdot}019$, this occurred at $Ra^2A^3 \approx 10^9$.

4. Experimental results for the end regions

Throughout the experimental programme attention was focused on the hot half of the cavity. However, to test further for heat losses from the walls of the tank a check on the symmetry about the centre-point of the cavity was made. Results from four representative measuring stations in the cold half of the cavity were included. A typical symmetry check, for experiment 2, is shown in figure 6, where the temperature is plotted as a function of depth for the various stations throughout the length of the cavity. To aid comparison of the temperature

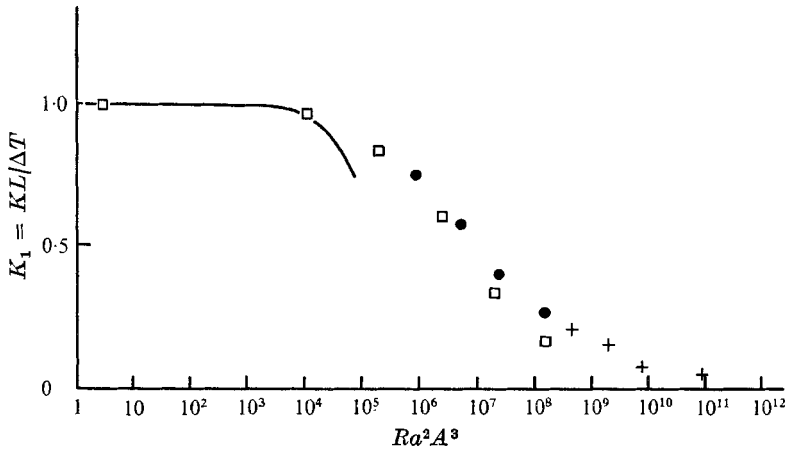

FIGURE 5. The non-dimensional average central temperature gradient *vs.* the transition parameter Ra^2A^3. ——, theoretical curve from part 1; □, values computed numerically in part 2; ●, experimental values, $A = 10^{-2}$; +, experimental values, $A = 1{\cdot}9 \times 10^{-2}$.

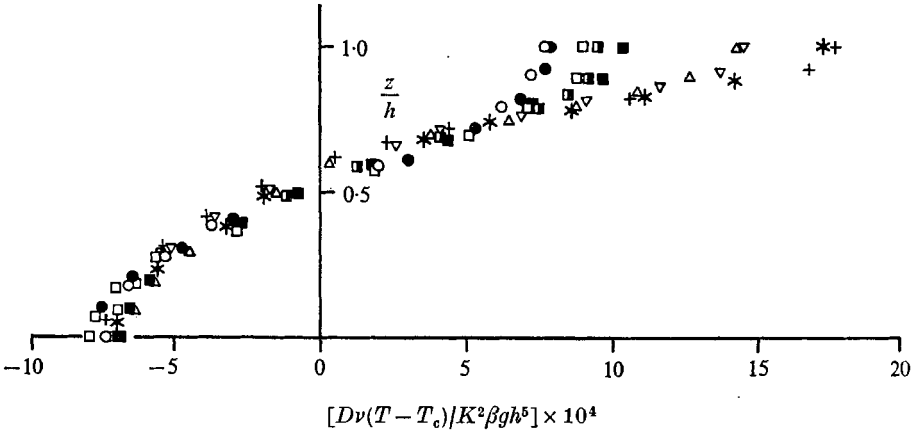

FIGURE 6. Experiment 2: vertical distance above the cavity bottom *vs.* non-dimensional temperature for various stations along the cavity. The values from the cold half of the cavity have been inverted to check the symmetry of the flow.

	+	×	▽	△	□	■	○	●	◑
Station	12	1	8	2	7	3	5	5	4
Distance from centre towards hot end (cm)	124·1	—	119·0	—	99·1	—	43·7	5·4	—
Distance from centre towards cold end (cm)	—	123·7	—	118·0	—	90·2	—	—	41·7

readings, the measurements from cold half of the cavity have been inverted to conform with those at the hot end.

As has already been mentioned, the experiments covered a range of the parameter Ra^2A^3 in which the flow changes from that described in part 1, where the flow in the core region is parallel and is driven by a longitudinal temperature gradient, to one in which the end regions provide the driving force and the core flow acts as a conduit connecting the hot and cold end regions. Streamline

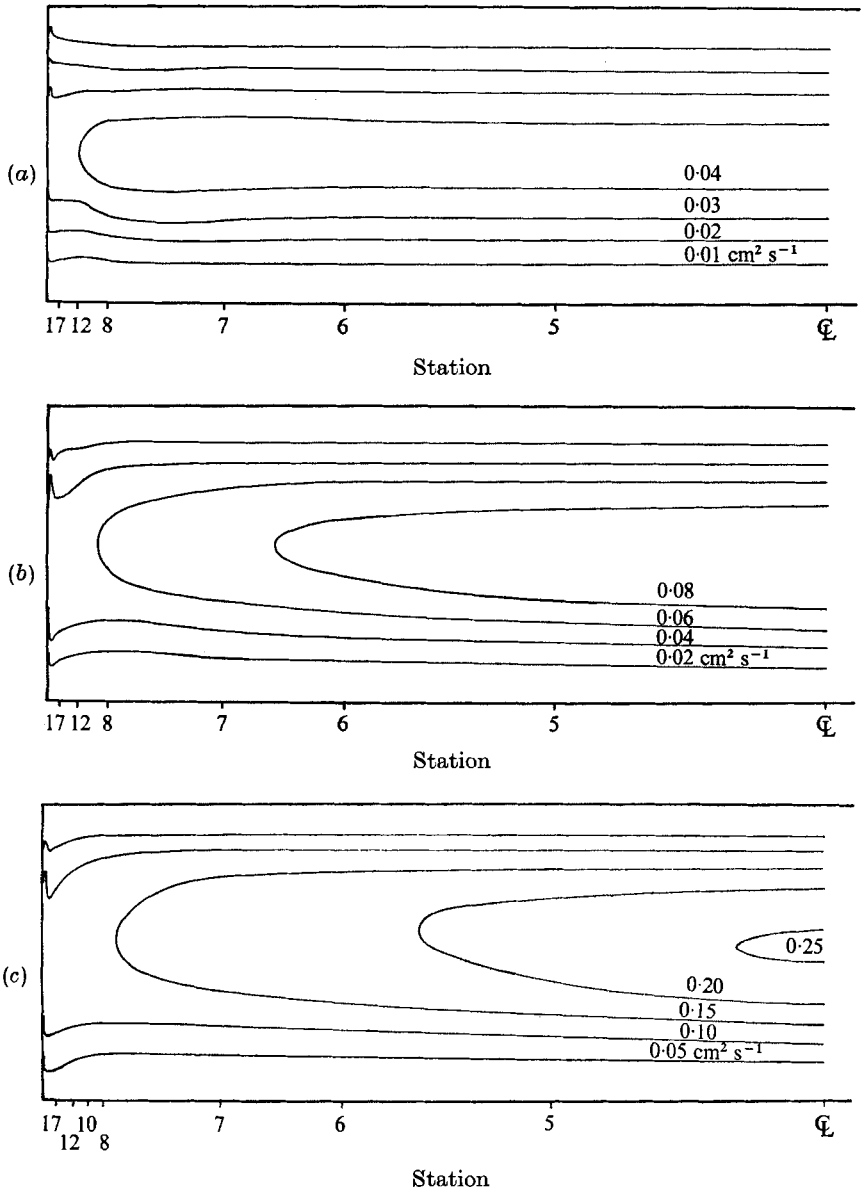

FIGURE 7. Streamlines. (*a*) Experiment 6: $Ra^2A^3 = 5{\cdot}50 \times 10^6$.
(*b*) Experiment 4: $Ra^2A^3 = 4{\cdot}35 \times 10^8$. (*c*) Experiment 3: $Ra^2A^3 = 8{\cdot}01 \times 10^{10}$.

patterns covering this transition are shown in figures 7 (*a*), (*b*) and (*c*). These are the results of experiments 6, 4 and 3. Results from the other experiments fall evenly in between those shown.

Quantitative comparison of actual streamlines and isotherms with those computed in part 2 was not possible because of the large cost of computing flows in which A is very small. However, inspection shows that most of the flow features mentioned in part 2 were also qualitatively present in the experimental flows.

A comparison of the temperature variations shown in figure 2 and the corresponding streamlines in figure 7 reveals that an increase in the amount of return flow outside the narrow wall layers occurs as the departure from a linear longitudinal temperature gradient increases. In figure 7(*a*), $Ra^2A^3 = O(10^6)$ and no streamlines close in the core region except for a mild maximum in the stream function located between stations 7 and 8. The transition from figure 7(*a*) to figure 7(*c*) shows that, as Ra^2A^3 increases, the core flows recedes from the ends to the central part, the stream-function maximum moves to the centre, and the return flow sets in where the longitudinal temperature gradient ceases to be linear. This behaviour is, at least qualitatively, analogous to the results found in part 2 for much larger aspect ratios. In figure 7(*c*), which shows the flow when Ra^2A^3 has become nearly 10^{11}, the mid-depth becomes an isotherm and there is a slow central circulation throughout the whole cavity, with about half the flow from the central part being turned around before it reaches the end boundary layer. It is interesting to compare this observation with work done for much larger aspect ratios. Figure 2(*a*) in part 2 shows a flow for an aspect ratio of one and a value of Ra^2A^3 of the order of 10^{10}. Here this slow core circulation is absent. Furthermore, Quon (1972), who studied flows for a unit aspect ratio and for values of Ra^2A^3 as large as 10^{12}, reported no return flow in the core. Elder's (1965) results are for $A = O(10)$ and $Ra^2A^3 = O(10^{20})$ and again they show no core return flow; all the fluid returns through a small vertical wall boundary layer. Unfortunately, the Rayleigh number could not be increased further in the present experiments and therefore it is still uncertain whether increasing Ra^2A^3 leads from a state of parallel core flow to a flow with vertical circulation, and then back to parallel core flow, the aspect ratio determining only the extent of the core return flow and the value of Ra^2A^3 at which this occurs, or whether the limit $Ra \to \infty$ is different for A small and A large. In this respect, the theory developed in part 1 for small values of Ra^2A^3 is also inappropriate since it predicts parallel flow in the core region for all values of the Rayleigh number. The limit $Ra \to \infty$ is, of course, complicated by the onset of instabilities of the type discussed by Hart (1972).

5. Heat transfer

The transfer of heat from the hot side wall to the opposite cold wall is obtained by looking at the Nusselt number $[(-L/\Delta T)\,dT/dx]_{x=0}$ associated with the flow. L is the correct length scale here, as we are dealing with the limit $A \to 0$, for which it was shown in part 1 that the temperature gradient is, to first order, equal to $\Delta T/L$. Thus the average Nusselt number $\overline{Nu}$ of the plate is equal to

$$\overline{Nu} = -(\Delta T A)^{-1} \int_0^h \left.\frac{dT}{dx}\right|_{x=0} dz,$$

but, by conservation of heat, this is equal to

$$(\Delta T A D)^{-1} \int_0^h (uT - DT_x)\,dz.$$

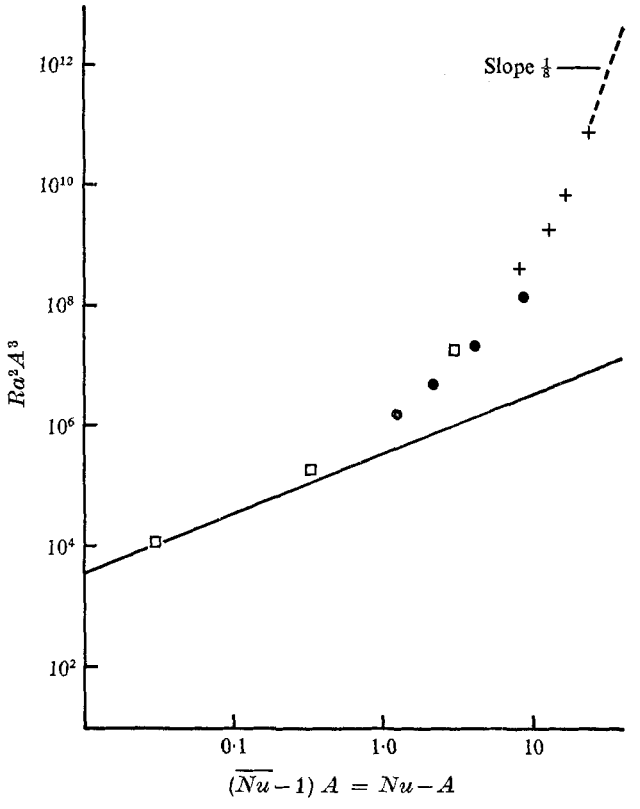

FIGURE 8. Heat transfer from the hot to the cold plate *vs.* the parameter Ra^2A^3. ——, theoretical curve from part 1; □, values computed numerically in part 2; ●, experimental values, $A = 10^{-2}$; +, experimental values, $A = 1{\cdot}9 \times 10^{-2}$.

The integral may be taken over any vertical cross-section and in particular the central cross-section. In part 1 it was shown that for Ra fixed and $A \to 0$

$$\overline{Nu} \sim Ra^2A^2 + 1$$

and by contrast when A is fixed and $Ra \to \infty$

$$\overline{Nu} \sim A^{-1}Ra^{\frac{1}{4}}.$$

For convenience in both comparison with part 2 and plotting the data, the above Nusselt number was evaluated at the central cross-section for each experiment and plotted in the form $\overline{Nu}A - A$ *vs.* Ra^2A^3. In this way the second limiting case has, for fixed A, a constant slope of $\frac{1}{8}$ on a log–log plot. In part 2 $A\overline{Nu}$ was designated by Nu. In the reduction of the experimental results the convective heat transfer far exceeded the conduction of heat. This is further evidence that the parallel core flow persists for values of Ra^2A^3 far larger than those required for domination of the heat transfer process by conduction. As pointed out in §3, the situation is quite similar to the enhanced longitudinal dispersion of a solute in pipe flow found by Taylor (1954).

The data shown on figure 8 are the results of all three parts of this study. The solid lines shows the asymptotic heat transfer for small values of Ra^2A^3 and both the numerical and experimental results indicate the strong convergence to the theory as Ra^2A^3 becomes less than about 10^6. The results for values larger than 10^7 show the convergence to the other limit, namely that

$$A\overline{Nu} = (Ra^2A^3)^{\frac{1}{8}}A^{-\frac{3}{8}}.$$

For the experimental data plotted the values of A are 10^{-2} and $1{\cdot}9 \times 10^{-2}$ and hence projection of the asymptotes into the $\overline{Nu}A - A$ axis should be spaced in the ratio 2·65 : 1·10. This is confirmed by the data, although only marginally since more data would be required for the case $A = 10^{-2}$ to prove this conclusively. The results also clearly show that, the smaller A is, the larger Ra must be to bring about a heat transfer coefficient characteristic of a $Ra^{-\frac{1}{4}}$ wall-boundary-layer thickness.

This investigation was carried out while the author was a visitor at the W. M. Keck Laboratory of Hydraulics and Water Resources, California Institute of Technology. The work was supported in part by National Science Foundation Grant GK-35774X.

REFERENCES

BAKER, D. J. 1966 *J. Fluid Mech.* **26**, 573–575.
CORMACK, D. E., LEAL, L. G. & IMBERGER, J. 1974 *J. Fluid Mech.* **65**, 209.
CORMACK, D. E., LEAL, L. G. & SEINFELD, J. H. 1974 *J. Fluid Mech.* **65**, 231.
ECKERT, E. R. G. & CARLSON, W. O. 1961 *Int. J. Heat Mass Transfer*, **2**, 106–120.
ELDER, J. W. 1965 *J. Fluid Mech.* **23**, 77–98.
FISCHER, H. B. 1972 *J. Fluid Mech.* **53**, 671–687.
GILL, A. E. 1966 *J. Fluid Mech.* **26**, 515–536.
HART, J. E. 1971 *J. Fluid Mech.* **47**, 547–576.
HART, J. E. 1972 *J. Atmos. Sci.* **29**, 687–697.
JANNOT, M. & MAZEAS, C. 1973 *Int. J. Heat Mass Transfer*, **16**, 81–100.
LOGAN, W. B. & CEBULSKI, D. E. 1970 *Am. Ass. Petroleum Geol. Mem.* no. 13.
QUON, C. 1972 *Phys. Fluids*, **15**, 12–19.
TAYLOR, G. I. 1954 *Proc. Roy. Soc.* A **223**, 446–468.